Bio-Design and Manufacturing (2022) 5:233–248
https://doi.org/10.1007/s42242-022-00184-5

RESEARCH ARTICLE

Adhesion-enhancing coating embedded with osteogenesis-promoting PDA/HA nanoparticles for peri-implant soft tissue sealing and osseointegration

Tingshu Su[1,2,3] · Ao Zheng[1,2,3] · Lingyan Cao[1,2,3] · Lingjie Peng[1,2,3] · Xiao Wang[1,2,3] · Jie Wang[1,2,3] · Xianzhen Xin[1,2,3] · Xinquan Jiang[1,2,3]

Received: 23 July 2021 / Accepted: 11 January 2022 / Published online: 19 February 2022

Abstract

Following dental implantation, the characteristic bacterial milieu of the oral cavity may lead to peri-implant inflammation, which can negatively impact osseointegration and cause implant failure. To improve soft tissue sealing around the implant, enhance osseointegration, and improve implant success rates, this paper proposes a composite multifunctional coating (PHG) prepared using gelatin and polydopamine/hydroxyapatite nanoparticles, investigates the effects of this novel coating on cell adhesion, proliferation, antibacterial activity, osteogenic differentiation, and evaluates its immune-related properties. The PHG coating was proved to have satisfactory hydrophilicity and wettability for cell attachment. Furthermore, it improved the expression of adhesion-related genes and proteins in human gingival fibroblasts, indicating its adhesion-promoting effect. Additionally, bone marrow mesenchymal stem cells exhibited strong osteogenic differentiation potential and mineralization on PHG-coated surfaces. Notably, the PHG coating exhibited antibacterial activity against *Streptococcus mutans*, as well as anti-inflammatory effects, potentially via the regulation of macrophages. Therefore, the proposed PHG coating may promote soft tissue sealing and bone bonding, providing a potential strategy for the surface modification of dental implants.

Keywords Dental implantation · Multifunctional coating · Titanium · Osseointegration · Soft tissue sealing

Introduction

With the significant technological advances of recent decades, dental implantation has transformed into a successful and routine treatment for dentition defects and edentulousness. Bone integration is a crucial aspect of successful dental implantation; therefore, peri-implant inflammation, as a biological complication affecting the bone integration of implants, has become an important research topic. Peri-implant inflammation causes the loss of bone support around the implant, which may lead to direct implantation failure, leading to economic losses and adverse effects [1–3].

Most dental implants are composed of titanium-based materials. Titanium is widely used in the production of implants due to its high biocompatibility. However, it is an inert metal with poor biological activity that does not support bone integration around the implant. Therefore, the osteogenic activity of titanium-based implants must be enhanced by surface modification. Specifically, the treatment of metal surfaces with alkali substances has been shown to improve the bone binding capacity through increasing the number of microspores on the metal surface and by altering the specific chemical properties of the metal [4]. Following alkali heat treatment, deposition of hydroxyapatite (HA) onto the titanium metal surface is challenging [5, 6], and an inorganic substance with similar properties to apatite in the natural bone matrix is often employed for inert metal-

Tingshu Su and Ao Zheng have contributed equally to this work.

✉ Xianzhen Xin
kristyxxz@126.com

✉ Xinquan Jiang
xinquanjiang@aliyun.com

1 Department of Prosthodontics, Shanghai Ninth People's Hospital, Shanghai Jiao Tong University School of Medicine, Shanghai 200011, China

2 College of Stomatology, National Center for Stomatology, National Clinical Research Center for Oral Diseases, Shanghai Jiao Tong University, Shanghai 200011, China

3 Shanghai Key Laboratory of Stomatology, Shanghai Engineering Research Center of Advanced Dental Technology and Materials, Shanghai 200011, China

lic implant biofunctionalization. In addition, the HA coating of implants gradually dissolves after being soaked in biological solutions, thus affecting the implant–bone bonding [7–9]. Therefore, it is of utmost importance to develop strategies to improve the interface bonding between HA coating and implant, thereby increasing the osteogenic activity of implants.

Marine muscles strongly adhere to hard rock surfaces via a bundle of foot filaments (byssus), which have been found to attach to nearly all surfaces (including superhydrophobic surfaces), showing remarkable adhesive and mechanical properties [10]. Polydopamine (PDA), a key component of the mussel byssus, has excellent biocompatibility and is widely used in the surface modification of biomedical materials. The main functional groups of polydopamine are amide and imide groups, which improve the surface properties of biomedical materials by covalently binding target molecules and functional metal ions [11]. Thus, exploiting the adhesion mechanism of the mussel byssus potentially improves the binding between the implant surface and the coating.

Moreover, the complex oral cavity environment contains bacteria that can induce peri-implant inflammation, resulting in the destruction of the biological seal between the oral soft tissue and the implant [10, 12]. It is therefore imperative to ensure that a strong soft tissue seal is created around the implant. Naturally, the epithelium and fibrous tissue form a strong soft tissue seal around the teeth. Hence, the ideal interface between implant and soft tissue should mimic the attachment of periodontal tissue to natural teeth, forming a tight "cuff'" to become a functional biological seal that can serve as a barrier to repel bacteria and other inflammatory factors. Gelatin, a macromolecular hydrophilic polymer, is a product of partial collagen hydrolysis that has been widely applied in the field of medicine due to its biodegradability, biocompatibility, and film-forming properties. In addition, it can promote cell adhesion to material surfaces [13–16].

In this study, a composite multifunctional coating was prepared to modify the properties of the titanium surface (Fig. 1). A porous structure was formed on the metal surface by alkali heat treatment. Subsequently, HA particles were adhered to the titanium surface via PDA to form a dense nano-HA biofilm, which was then coated with gelatin to enhance its biological sealing effect. Subsequently, the influence of the obtained composite multifunctional coating on cell adhesion, proliferation, antibacterial activity, osteogenic differentiation, and immune-related properties was investigated. We aimed to optimize the design of the new implant surface modifications and develop a novel method to improve the osseointegration and biocompatibility of titanium implants.

Materials and methods

Materials

Commercial pure titanium foils (0.25 mm thick, 99.5% purity) were purchased from Alfa Awsar Co., Ltd. (Tianjin, China). HA, dopamine (DA), and gelatin were acquired from Aladdin Industrial Co., Ltd. (Shanghai, China). CCK-8, alkaline phosphatase (ALP), and bicinchoninic acid (BCA) assay kits were obtained from Beyotime Biotechnology Co., Ltd. (Jiangsu, China). FITC-phalloidin and DAPI were purchased from Invitrogen (Carlsbad, CA, USA). Fetal bovine serum (FBS) was obtained from Gibco (USA). DMEM and 100 U/mL penicillin and streptomycin were purchased from Hyclone (South Logan, USA). Dispase II solution was obtained from Roche (Basel, Switzerland).

Preparation of PDA-HA-Gelatin@Ti (PHG@Ti)

Pure Ti foils (Group 1) were soaked in 5.0 M NaOH aqueous solution at 60 °C for 24 h, gently washed with distilled water, and dried at 40 °C for 24 h at room temperature. The foils were subsequently heated to 600 °C at a rate of 5 °C/min in an electric furnace and held for 1 h before cooling down to room temperature. The samples were then covered with

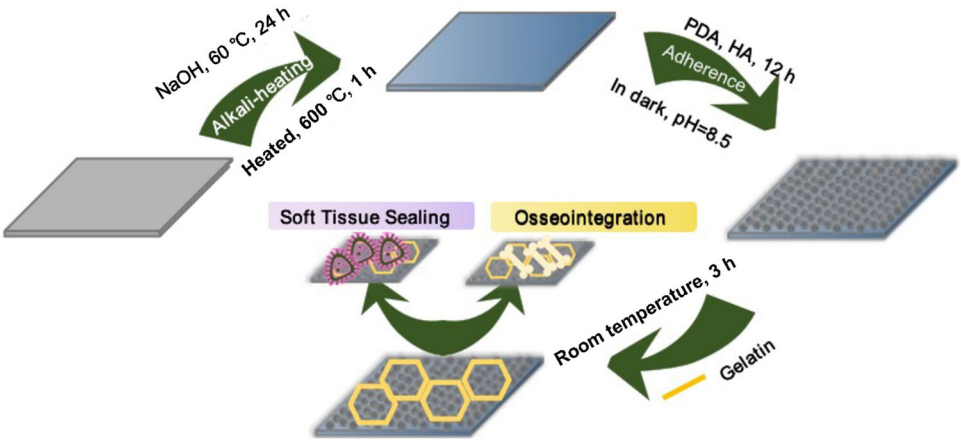

Fig. 1 Schematic illustration of the preparation process of PHG coating on the pure titanium surface

PDA by incubation with 2 mg/mL DA in Tris–HCl buffer solution (pH: 8.5) for 12 h in the dark. The PDA-coated Ti foil (P@Ti, Group 2) samples were rinsed with deionized water and washed under ultrasonic conditions for 15 min.

After alkali heat treatment, the foils were immersed in 2 mg/mL DA and 1 mg/mL nHA solution prepared with Tris–HCl buffer (pH: 8.5). After 16 h, the samples were ultrasonically washed for 15 min and dried to create HA-PDA-coated Ti foils (PH@Ti, Group 3). Next, gelatin was prepared with deionized water to form a 3% solution. The cleaned PH@Ti foils were placed in a 12-well cell culture plate, to which 1 mL of 3 wt.% gelatin solution was added, followed by immersion at room temperature for 3 h. The PH@Ti foils modified with gelatin were soaked in deionized water and washed on a shaker thrice to remove unfixed gelatin to form the PHG@Ti (Group 4) sample.

Surface characterization

The surfaces of Ti, P@Ti, PH@Ti, and PHG@Ti were observed using scanning electron microscopy (SEM; Phenom™ Pharos, Thermo Fisher Scientific, Waltham, MA, USA). The elemental composition of the coating and its distribution were further examined using energy-dispersive spectroscopy (EDS; Phenom™ Pharos, Thermo Fisher Scientific, Waltham, MA, USA). The surface chemistry of the samples was characterized by X-ray photoelectron spectroscopy (XPS). The water contact angle was measured to determine the wettability of the samples (Model 200, Future Scientific, Taiwan, China). Moreover, the FTIR spectra were measured with an FTIR spectrophotometer (Nicolet 5DXC spectrometer, Thermo Fisher Scientific, Waltham, MA, USA) using a KBr pellet (10 mm in diameter). The spectra were examined within a wave range of 3000–500 cm^{-1}.

Photothermal effects of modified samples

The photothermic ability of Ti, P@Ti, PH@Ti, and PHG@Ti was characterized with an infrared thermal imaging system. Briefly, the samples (10 mm × 10 mm) were placed in a 24-well culture plate under wet conditions (0.5 mL PBS) and irradiated by an 808 nm laser beam (diameter: 15.6 mm, 0.5 W/cm^2) for 1, 2, 5, and 10 min. The temperature and thermal images were recorded.

In vitro biological evaluation

All experimental protocols involving animals were approved by the Institutional Animal Care and Use Committee and followed the procedure for Animal Experimental Ethical Inspection of the Ninth People's Hospital, which is affiliated with Shanghai Jiao Tong University School of Medicine.

With the consent of the ethics committee of the Ninth People's Hospital affiliated with the Medical College of Shanghai Jiao Tong University and the informed consents of the patients, the healthy gingival tissues removed during the extraction of mandibular third molars were collected for the study.

Extraction and culture of rat bone marrow mesenchymal stem cells (BMSCs) and human gingival fibroblasts (HGFs)

BMSCs were isolated from 4-week-old Sprague–Dawley rats (Shanghai SLAC Experimental Animal Center, Shanghai, China). The femur was separated by cutting at the epiphysis after the rats were intraperitoneally injected with pentobarbital for euthanasia. Bone marrow was flushed rapidly using DMEM supplemented with 10% FBS, 100 U/mL penicillin and streptomycin, and collected by centrifugation. The harvested cells were incubated in DMEM at 37 °C in a humidified air/5% CO_2 atmosphere. The culture medium was changed every 3 days.

The gingival tissue was rinsed with PBS containing 10% penicillin until the rinse solution became colorless and transparent, then immersed in dispase II solution at 4 °C overnight. The gingival connective tissue was then cut into 1–2 mm^3 pieces and cultured in 5 mL of DMEM containing 10% FBS. The solution was changed every 2 days, and the cells were passaged when 80% cell fusion was achieved after 14–18 days. The HGFs used in the experiment were derived from the second to the fourth passage of cultured cells.

Cell viability and proliferation experiment

The cells were seeded onto Ti, P@Ti, PH@Ti, and PHG@Ti at a density of 5×10^3 cells/foils ($d = 0.5$ cm). Following to the manufacturer's protocol, after 1, 3, and 7 days of culture, the medium was exchanged with fresh medium containing CCK-8 reagent (Dojindo, Kumamoto, Japan), followed by incubation at 37 °C for 1.5 h. The absorbance of the solution at 450 nm was measured using a microplate reader (Tecan Spark, Switzerland). Cells seeded on the plate were used as the control group (TCP).

The cells were seeded at a density of 1×10^5 cells/foils ($d = 1$ cm). After 24 h of culture, a Calcein-AM/propidium iodide (PI) double stain kit (Yeasen, China) was used to perform the live/dead cell assay. The stained cells were observed using laser scanning confocal microscope (LSCM; Leica, Wetzlar, Germany).

Cell adhesion and extension

The effect of Ti, P@Ti, PH@Ti, and PHG@Ti samples on cell adhesion and extension was investigated by visualizing the BMSCs and HGFs seeded onto the surfaces of

Table 1 Primers used for PCR in HGFs

Gene	Forward primer sequence (5′–3′)	Reverse primer sequence (3′–5′)
GAPDH	TGCACCACCAACTGCTTAGC	GGCATGGACTGTGGTCATGAG
Integrin $\alpha 3$	CATCCTCCTGCTGTGGAAGT	CGGTCAGCCTCTCTGTCTCT
Integrin $\beta 1$	TACTTGTGAAGCCAGCAACG	ACAGACACCAAGGCAGGTCT
Vinculin	GCTGCCAGTTCTCATTTCAGC	ATGGCTTCAGTGTCCTTGCT
Col-1	TGTTCAGCTTTGTGGACCTC	CTTGGTCTCGTCACAGATCA

Table 2 Primers used for PCR in BMSCs

Gene	Forward primer sequence (5′–3′)	Reverse primer sequence (3′–5′)
GAPDH	GGCAAGTTCAACGGCACAG	CGCCAGTAGACTCCACGACAT
ALP	TCACTTCCGCCCGGAACCCT	TGTCCTGCCGGCCCAAGAGA
BMP2	TGGGTTTGTGGTGGAAGTGGC	TGGATGTCCTTTACCGTCGTG
OCN	GCCCTGACTGCATTCTGCCTCT	TCACCACCTTACTGCCCTCCTG
RUNX-2	ATCCAGCCACCTTCACTTACACC	GGGACCATTGGGAACTGATAGG

different groups at a density of 2×10^5 cells/sample (d = 1 cm). After 6 h of incubation, all samples were removed and fixed with 4% glutaraldehyde at room temperature for 15 min. The dried samples were observed for adhesion through SEM. Moreover, cell morphology was observed using LSCM. After 6 h of cell culture, the samples were immersed in 4% paraformaldehyde (PFA) and incubated with FITC-phalloidin for 1 h at 37 °C to observe the cytoskeleton, and subsequently incubated with DAPI for 10 min to observe the nuclei.

In order to assess the soft tissue sealing effect in vitro, HGFs were cultured on each sample for 1 and 3 days. RT-PCR was then employed to assess the mRNA levels of integrin $\alpha 3$, integrin $\beta 1$, vinculin, and Col-1. The gene expression data were analyzed using the $2^{-\Delta\Delta CT}$ method. The relevant primer sequences are listed in Table 1.

Immunofluorescence staining

The bone-specific protein, OCN, and adhesion-related protein, integrin-α, were subjected to immunofluorescence staining using a previously described method [17]. BMSCs and HGFs were seeded onto the surfaces of Ti, P@Ti, PH@Ti, and PHG@Ti samples at a density of 2×10^5 cells/sample (d = 1 cm).

The BMSCs were cultured on the samples for 7 days and then fixed in 4% PFA solution. The samples were then treated with mouse monoclonal anti-OCN primary antibody (Servicebio Technology Co. Ltd., Wuhan, China) and Alexa Fluor 594-conjugated secondary antibody.

The HGFs were cultured on the samples for 1 day and then fixed in 4% PFA solution. The samples were treated with mouse monoclonal anti-integrin-α primary antibody (Servicebio Technology Co. Ltd.) and Alexa Fluor 594-conjugated secondary antibody.

Moreover, FITC-phalloidin and DAPI staining were performed on both BMSCs and HGFs, and the results were observed under LSCM.

Osteogenic gene expression of BMSCs

The BMSCs were cultured on the samples for 3, 7, and 14 days. The total RNA of the BMSCs was then harvested using TRIzol (Sigma-Aldrich, USA). The cDNA was produced by RNA extraction using a synthesis kit (Takara Bio, Shiga, Japan), and these cDNA sequences were used for RT-PCR to assess the mRNA levels of BMP2, OCN, RUNX-2, ALP and GAPDH. The gene expression data were analyzed using the $2^{-\Delta\Delta CT}$ method [18]. The relevant primer sequences are listed in Table 2. All gene expression data were normalized to the GAPDH reference gene and denoted as the fold ratio of the Ti samples.

ALP activity assay and calcium deposition assay

The BMSCs were seeded onto the surfaces of different samples at a density of 2×10^5 cells/sample (d = 1 cm). On days 7 and 14, each sample was rinsed thrice with PBS and fixed with 4% PFA for 15 min. According to the manufacturer's instructions, the cells were subjected to ALP staining (Beyotime, Shanghai, China) after washing twice with distilled water. For ALP semi-quantitative analysis, a BCA kit (Thermo Fisher Scientific, Waltham, MA, USA) and an ALP kit (Beyotime, China) were used according to the manufacturer's instructions. The final ALP activity was presented as OD values per milligram of total protein at 405 nm.

On day 21, the fixed cells were stained with 1% Alizarin red (Sigma-Aldrich) for 10 min, and then rinsed with water. The nuclei were counterstained with DAPI, and calcium deposition was observed using LSCM. After alizarin red

Table 3 Primers used for PCR in macrophages (RAW 264.7 cells)

Gene	Forward primer sequence (5′–3′)	Reverse primer sequence (3′–5′)
iNOS	TCTCAAACTGCTCTGAGGTG	CGTTGGATTTGGAGCAGAAGTG
IL-1b	AACCTGCTGGTGTGTGACGTTC	CAGCACGAGGCTTTTTTGTTGT
IL-10	GCCAGAGCCACATGCTCCTA	GATAAGGCTTGGCAACCCAAGTAA
TGF-β	TAATCGTGAATCAGGCAG	ATCCATCACTAGATCGCCCT

staining, 10% cetylpyridine chloride was added and cells were incubated at room temperature for 30 min. The OD value at 562 nm was determined and used for the semi-quantitative analysis of calcium deposition [19].

In vitro antibacterial activity

Bacterial culture A *Streptococcus mutans* (UA159) [20] strain was cultivated in tryptic soy broth (TSB) and agar (TSA). The bacteria were collected and centrifuged at 5000 r/min for 4 min and subsequently resuspended in saline. The different Ti foil samples were placed in 24-well plates and incubated in 1 mL of bacteria-containing medium (10^6 CFU/mL) under standard anaerobic conditions (80% N_2, 10% H_2, 10% CO_2 at 37 °C) for 24 h [21]. Afterward, all samples were irradiated by an 808 nm near-infrared (NIR) laser (diameter: 15.6 mm, 0.5 W/cm^2) for 5 min.

Bacterial viability experiment For the live/dead cell assay, the bacteria on all substrates were incubated with SYTO9 and PI stained after being cultured for 24 h at 37 °C. The live bacteria appeared green and the dead ones appeared red. The plates were observed using a fluorescence microscope (Olympus, Japan). The following formula was applied for calculating the antibacterial ratio:

$$C = A/(A + B) \times 100\%,$$

where C indicates antibacterial ratio, A is the average number of dead bacteria of each group (Ti, P@Ti, PH@Ti, and PHG@Ti), and B indicates the average number of live bacteria of each group (Ti, P@Ti, PH@Ti, and PHG@Ti). The images were recorded and analyzed to determine bacterial numbers using ImageJ software.

Immune response of macrophages

Macrophage culture and cell viability assay The murine macrophage cell line RAW 264.7 was cultured in DMEM medium supplemented with 10% FBS and 1% penicillin/streptomycin at 37 °C and 5% CO_2 in a humidified environment. After culturing for 24 h, cell proliferation was measured using the CCK8 assay kit (Dojindo, Kumamoto, Japan) using the same procedures as described in section "Cell viability and proliferation experiment".

Inflammation-related gene expression The expression levels of inflammation-related genes (*iNOS, IL-1b, IL-10, and TGF-β*) were determined using real-time RT-PCR using the same procedures as described in section "ALP activity assay and calcium deposition assay". The primer sequences are listed in Table 3.

Statistical analysis

All data ($n = 3$) obtained in this study were expressed as mean and standard deviation and were analyzed using GraphPad Prism (GraphPad Software, USA). The statistical comparisons were performed using one-way ANOVA and SNK. Any differences were considered statistically significant at $p < 0.05$.

Results and discussion

Physical properties and material characteristics

Figure 2a shows the morphology of different coatings on the pure titanium substrate; a porous structure was formed on the surface of the titanium sheet as a result of alkali heat treatment. PDA was observed on the porous titanium base surface after further PDA treatment. The needle/rod microcrystals were evenly distributed, indicating that HA was uniformly mixed into the coating. Moreover, the gelatin scaffold was formed on the surface of the titanium sheet, which did not affect the porous surface structure. The EDS elemental composition analysis indicated that the PH@Ti and PHG@Ti contained Ti, O, Ca, P, and C, while the PHG@Ti samples contained a higher elemental proportion of C (Fig. 2b).

The XPS revealed the surface chemical composition of Ti, P@Ti, PH@Ti, and PHG@Ti. Peaks of Ti, O, and C were observed on the Ti substrates (Fig. 3a). After self-polymerization of the PDA film on the titanium substrate, the peak strength of C1s increased. The XPS spectra of the samples with HA showed characteristic peaks of Ca and P (Fig. 3a). The C and O peaks changed after the addition of the gelatin stent. The XPS results revealed that the PHG coating was successfully prepared on the Ti substrate. Figure 3b shows the results of infrared spectra of Ti, P@Ti, PH@Ti, and PHG@Ti. Compared with the Ti sample, PH@Ti and

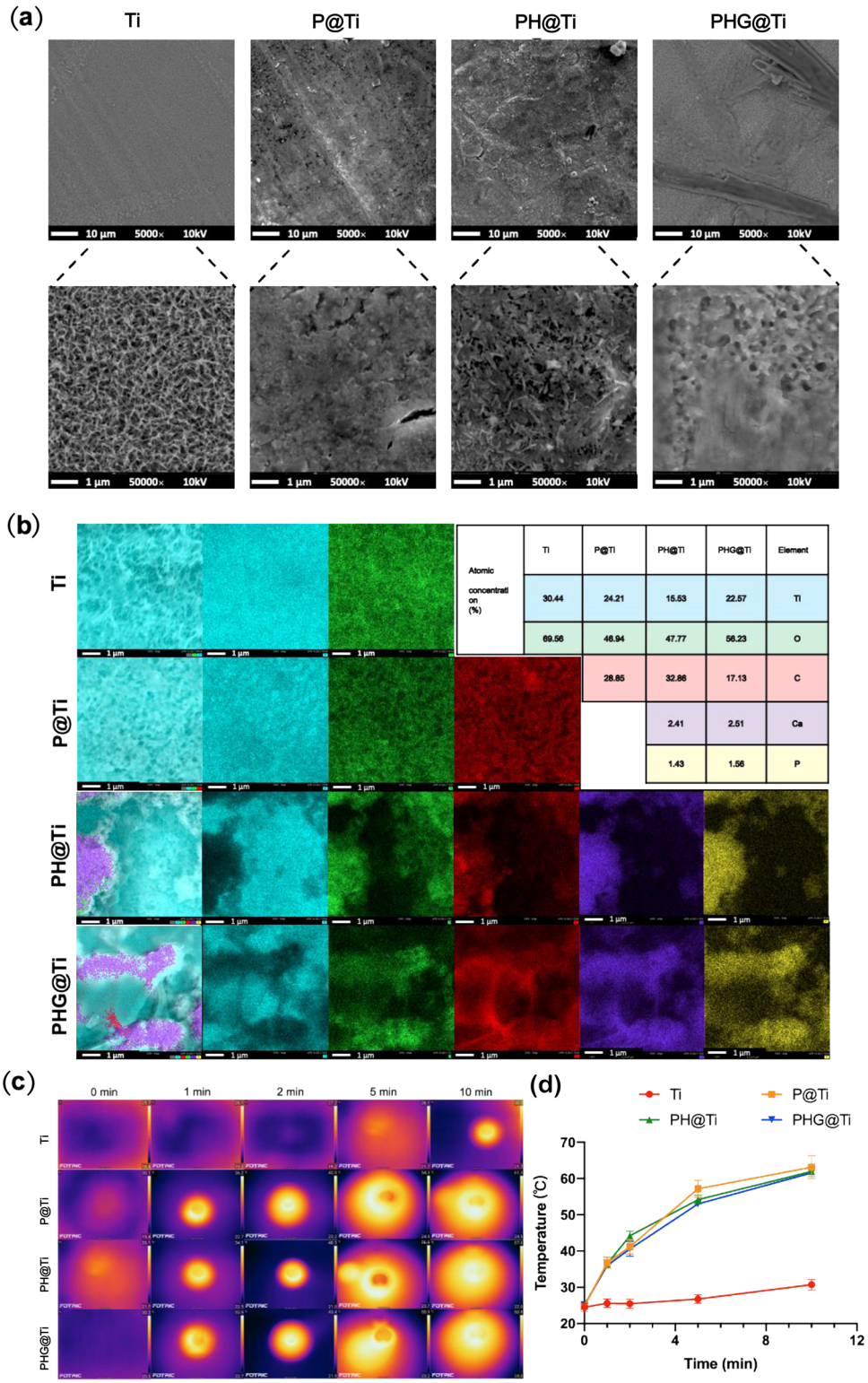

Fig. 2 Surface morphology tests. **a** SEM images and **b** EDS elemental analysis of the Ti, P@Ti, PH@Ti, and PHG@Ti samples. **c** Photographs and **d** statistics of photothermal detection of the Ti, P@Ti, PH@Ti, and PHG@Ti samples

PHG@Ti showing peaks at 3665 cm^{-1} were caused by O–H bonds [22]. In the P@Ti, PH@Ti, and PHG@Ti samples, the characteristic peak observed near 1618 cm^{-1} corresponds to the stretching vibration peak of the C = C bond in the benzene ring, while the 1221 cm^{-1} denotes the stretching vibration peak of the C–O bond in the catechol structure [23]. The spectra of PH@Ti and PHG@Ti showed new absorption peaks at around 1100 and 650 cm^{-1} due to the presence of phosphate radical, and it also showed similar peaks near 1350 cm^{-1} because of the formation of carbonate from hydroxyapatite.

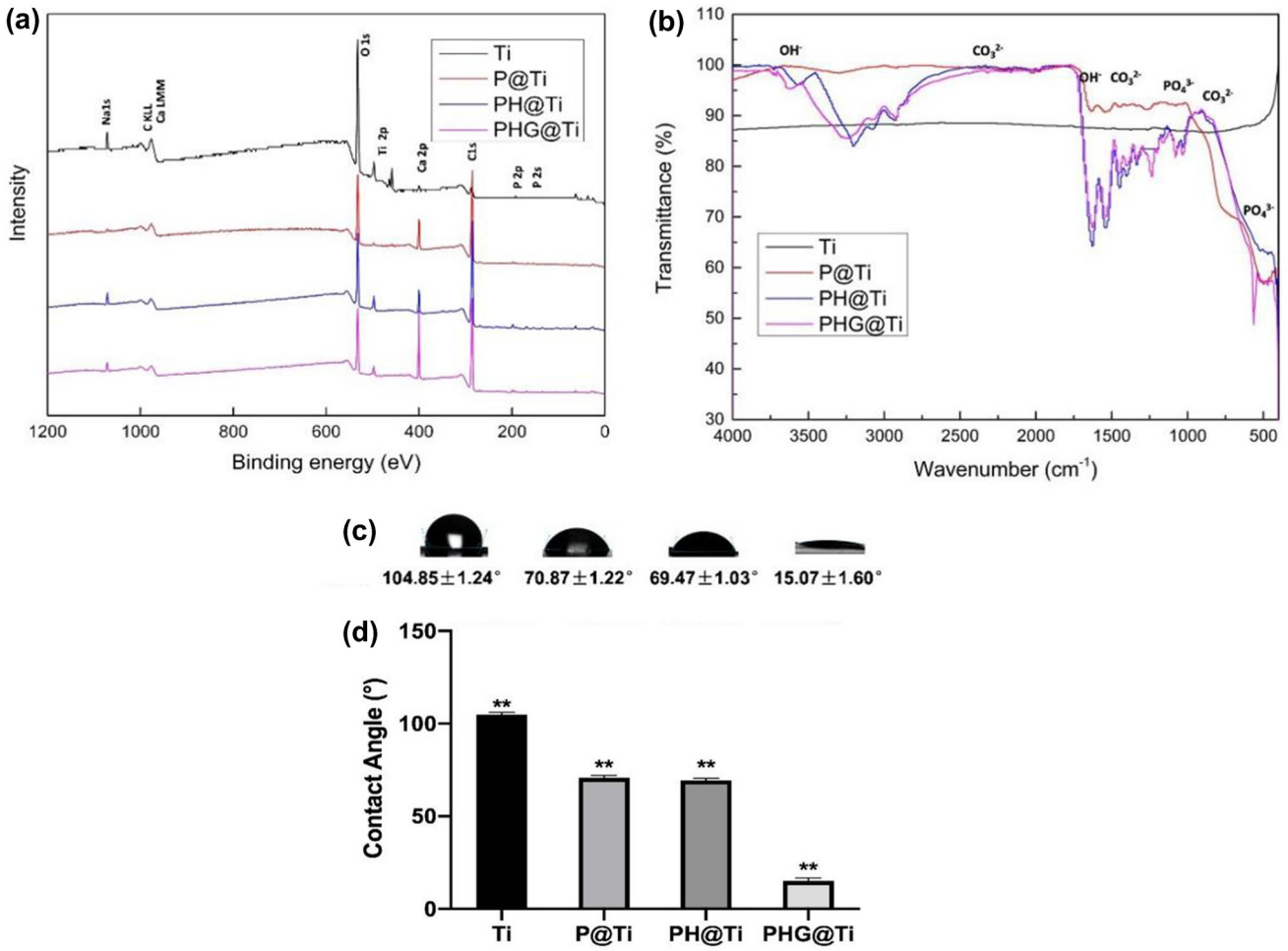

Fig. 3 Sample characteristics. **a** XPS and **b** FTIR spectroscopy results for the Ti, P@Ti, PH@Ti, and PHG@Ti samples. **c** Water droplets on different surfaces at room temperature. **d** Statistical analysis of contact angles of the coated groups (compared with the Ti group, * $p < 0.05$, ** $p < 0.01$)

In the PHG@Ti spectra, the absorption peak at 1550 cm^{-1} indicated the formation of amide bonds. The above results showed a clear presence of HA and gelation, which confirms that the PHG coating was successfully synthesized on the Ti surface.

The static contact angle was employed to reveal the change of hydrophilic/hydrophobic properties after each modification step (Figs. 3c and 3d). After hydrothermal treatment, the titanium base showed general hydrophilicity and its contact angle was 105°. Following PDA modification, the contact angle decreased due to the hydrophilicity of the PDA film, and it became hydrophilic with a contact angle of about 70°. As for the PH coating, the contact angle was about 69°, which was not significantly changed compared to that of PDA. However, the contact angle decreased significantly after the gelatin stent was reduced to 24°. Therefore, the PHG samples exhibited better wettability than the Ti substrate. Notably, the improved hydrophilicity of the Ti matrix modified by the PHG coating promoted the adhesion and osteogenesis of bone-related cells by increasing the affinity between cells and biomaterials.

Titanium is a stable inert metal and does not degrade in the biological environment of human body [24], so Ti is widely used as the substrate of implant. In this study, the novel coating consisting of PDA/HA/gelatin was soaked in degradation solution and the material degradation was evaluated. The results of ICP showed that there was no obvious Ti precipitation (Fig. S1 in Supplementary Information); with the progress of time, some Ca ions can be detected at 3w-4w, indicating that the coating is gradually biodegradable. The SEM results after soaking for 4w showed that some areas of the coating on the surface of titanium sheet could be degraded. 4w is also the early stage of bone tissue formation [25]. It can be expected that with the biodegradation of the implant surface coating, the surrounding tissue can grow and form a good bone bond.

In vitro photothermal investigation of PHG@Ti coating

In order to evaluate the photothermal performance of different samples, pure Ti, P@Ti, PH@Ti, and PHG@Ti were treated with 808 nm laser irradiation (0.5 W/cm^2) [26] for 1, 2, 5, and 10 min (Fig. 2c). The temperature of the PBS in the pure Ti group increased from 24.0 to 30 °C after irradiation (0.5 W/cm^2) for 600 s. However, the P@Ti, PH@Ti, and PHG@Ti groups rapidly increased from 24.0 to 63.1, 61.1, and 61.5 °C, respectively, indicating a marked photothermal effect. Meanwhile, the temperature changes for P@Ti, PH@Ti, and PHG@Ti were found to be time-dependent (Figs. 2c and 2d). That is, with the increase of time from 60 to 600 s, the temperature of PHG@Ti increased from 36 to 44, 54, and 61 °C. Moreover, as shown in Fig. 2d, the yellow central area was 1 cm × 1 cm in size in the PBS environment, indicating the homogeneous surface temperature of the PDA under NIR irradiation. This indirectly suggests that the coating on the material surface was well-distributed. Overall, these results confirmed that the homogeneous distribution of the PDA coating played a key role in endowing the samples with optimal photothermal properties.

In vitro biological activities

Cell morphology

Early cell adhesion and spreading is essential for subsequent cell growth, proliferation, and differentiation [27, 28]. In this study, cytoskeleton fluorescence staining of BMSCs and HGFs was performed after culturing for 6 h on different substrates, and the results are shown in Fig. 4. The cells combined well with the matrix and exhibited a typical osteoblast phenotype. The BMSCs and HGFs attached to the matrix had polygonal structures, showing filamentous foot and flaky foot extensions. The HGF adhesion test results also showed that the cells had certain directional growth ability after the addition of gelatin scaffold. Moreover, the arrangement was clear, and the contact between cells was straightforward. On the surface of the titanium base modified by PDA, the cells exhibited cytomegalic extensions. After adding the gelatin scaffold, the cells spread to the titanium matrix, with various observable cytoplasmic extensions and filopodia. Meanwhile, the cell distribution on the surface was more uniform. The results showed that the regular and dense needle/rod crystals enhanced the adhesion of cells to the surface, and gelatin provided a positive charge to the material surface, making it easier for the material to bind to integrin receptors on the cell membrane, thereby improving cell adhesion. Consequently, surface modification with PDA and gelatin improved the cell compatibility of the material. These results were consistent with the hydrophilic results: the increase in cell adhesion and proliferative ability on these surfaces was due to the hydrophilicity, which is the key factor in osteogenesis, directly affecting the subsequent biological behavior.

Cell viability and proliferation experiment

The activity of BMSCs and HGFs on the scaffolds was verified using a live/dead cell assay (Figs. 5a and 5b). After 24 h of culture on the four modified samples, most cells survived, indicating that none of the samples were cytotoxic.

Cell proliferation was evaluated using the cell counting kit-8 (CCK-8) assay (Figs. 5e and 5f). The results showed that, after four or seven days of growth, none of the Ti, P@Ti, and PH@Ti groups presented a significant difference compared with the control group (TCP). Meanwhile, cell viability was higher on the PHG@Ti sample compared to the pure Ti sample on day 7 ($p < 0.05$). This enhanced cellular compatibility of the modified Ti substrate was attributed to the immobilization of PDA and gelation, which improved the initial cell adhesion and proliferation. The survival rate of BMSCs and HGFs on the PHG-modified Ti matrix slightly increased, indicating that the immobilization of gelatin enhanced the cell compatibility of the modified matrix and promoted the adhesion and proliferation of BMSCs and HGFs. These results revealed that the four groups of Ti samples had good biocompatibility and lacked cytotoxicity.

Cell adhesion and extension

The fluorescence intensity following integrin-α staining in HGF cells after 3 days of culture differed among the four groups. That is, the abundance of integrin-α was the highest in the PHG@Ti group, while that of the P@Ti and PH@Ti coating groups was higher than that of the Ti group (Fig. 6d). These results confirmed the role of gelatin and PDA in promoting cell adhesion.

HGF cells were cultured on different coated surfaces for 3 days, and the expression of adhesion-related genes, including ITGA3, ITGB1, VCL, and Col-1 (Fig. 6f), was assessed. The expression of these genes was the highest in the PHG group, indicating that PHG had the best cell adhesion-promoting performance. Moreover, the expression of adhesion-related genes increased following PDA addition, which was closely related to the hydrophilicity of PDA and gelatin, as well as to the wettability of the material surface. This might have occurred because HA roughens the surface of the scaffold, making it easier for cells to adhere. In addition, the functional groups of PDA could interact with cells and promote cell viability [29]. Besides, the modification of Ti by gelation could further improve the biocompatibility of the scaffolds and promote cell adhesion and proliferation [30].

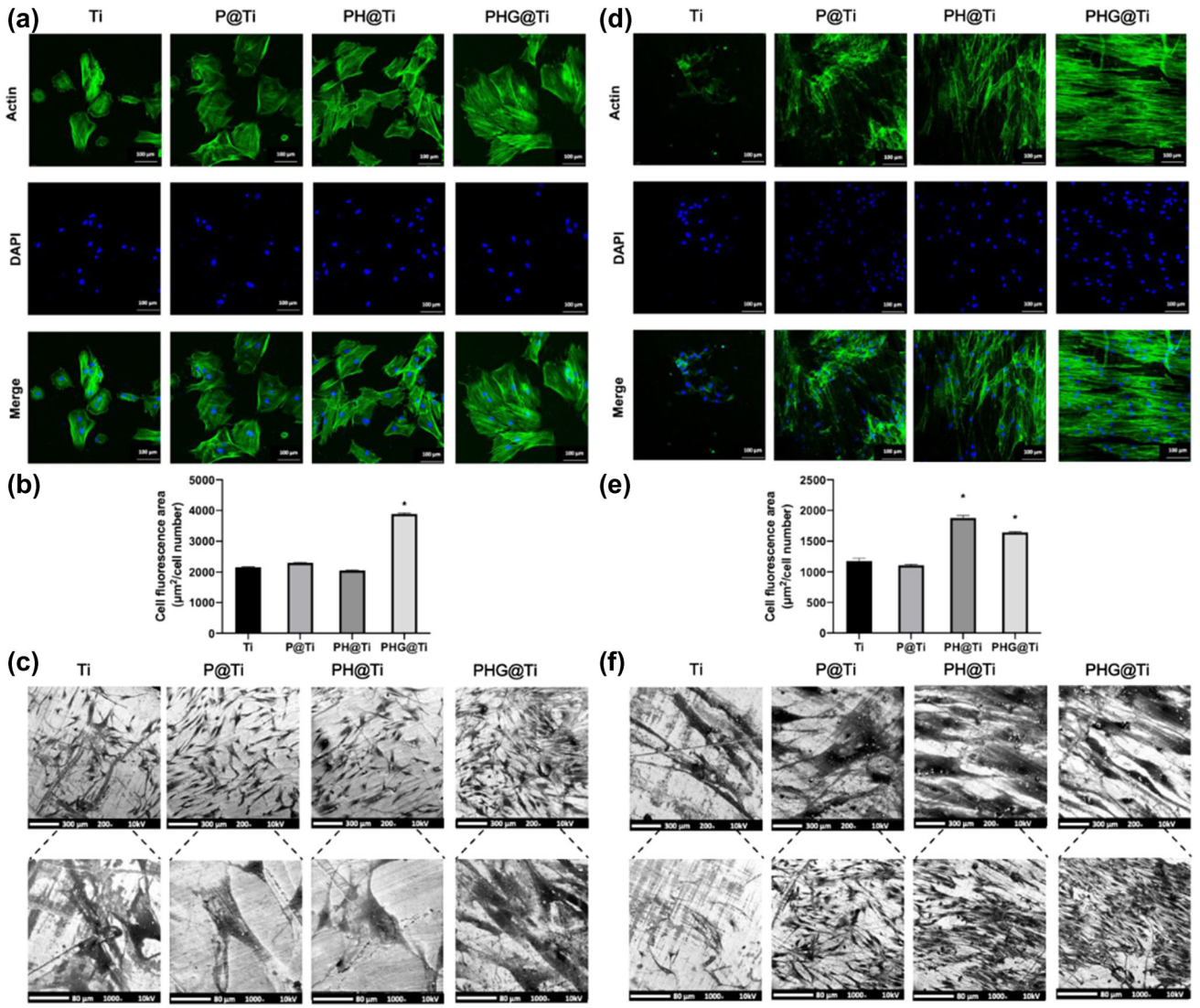

Fig. 4 Cell adhesion and extension assay. **a** Fluorescence staining, **b** statistics, **c** SEM for BMSCs cultured on different samples for 6 h., **d** Fluorescence staining, **e** statistics, and **f** SEM for HGFs cultured on different samples for 6 h. Scale bars = 100 μm (**a**) and (**d**), Scale bars = 300 μm in first row of (**c**) and (**f**), Scale bars = 80 μm in the second row of (**c**) and (**f**). (compared with the Ti group, * $p < 0.05$)

Cell differentiation and mineralization

The expression of osteocalcin (OCN) protein was detected by the fluorescence staining of BMSCs cultured on different coated surfaces for 7 days (Fig. 6a). The results of immunofluorescence assay showed that OCN protein expression was higher in the PHG@Ti and PH@Ti groups, whereas some OCN-positive cells were present in the P@Ti group, although the OCN expression was low. Thus, HA appears to have a certain osteogenic effect on BMSCs and can improve the expression of osteogenic proteins.

Regarding the relative gene expression of osteoblasts, the changes in osteogenic gene expression in BMSCs were examined during osteogenesis after 3, 7, and 14 days of culture (Fig. 6c). Several target markers, including BMP-2, OCN, Runx-2, and ALP, were analyzed, and their expression was found to be the highest in the PHG sample, indicating that PHG had the best osteogenic differentiation ability. Moreover, the osteogenic capacity of PDA and HA coating was higher than that of the Ti group. The results showed that HA and PDA had synergistic osteogenic effects under osteogenesis induction conditions. Adding gelatin improved the osteogenic performance, which may be related to the enhancement of cell adhesion. Meanwhile, HA could promote the osteogenesis and mineralization of BMSCs. In addition, PDA affects the enrichment of calcium ions [31, 32], and a high concentration of calcium can result in the formation of HA nucleation sites [33, 34], indicating that

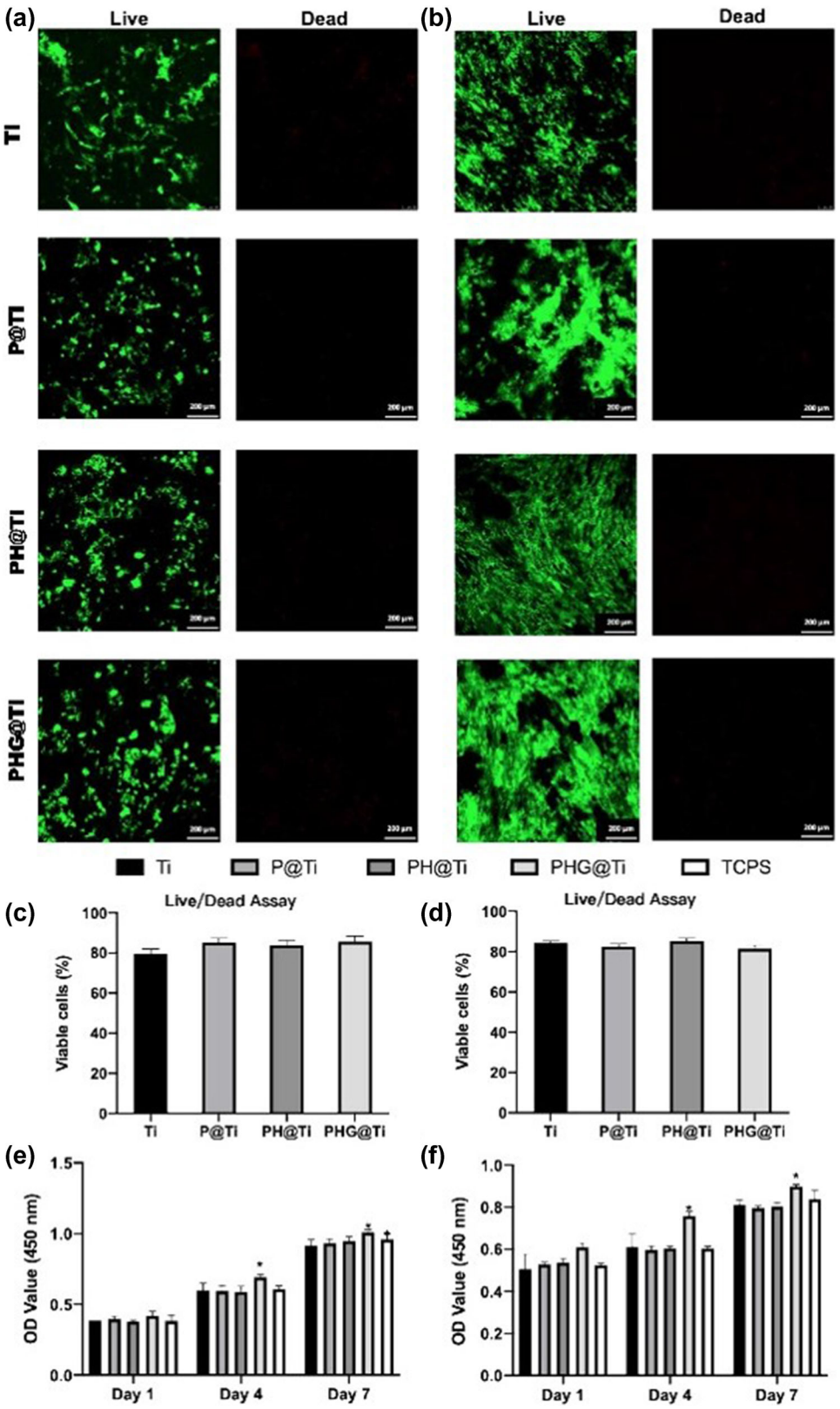

Fig. 5 Cell viability and proliferation experiment. Live/dead cell assay of **a** BMSCs and **b** HGFs seeded on the different samples. Live cells appeared green, whereas dead cells appeared red. Statistics of live/dead cell staining of **c** BMSCs and **d** HGFs. The CCK-8 assay of **e** BMSCs and **f** HGFs was performed after 1, 4, and 7 days of cell culture, and the results were analyzed using GraphPad Prism (* $p < 0.05$ compared with Ti)

PDA mineralizes the material surface. Therefore, the combined application of PDA, HA, and gelatin can improve the osteogenic and mineralization potential of this new composite multifunctional coating.

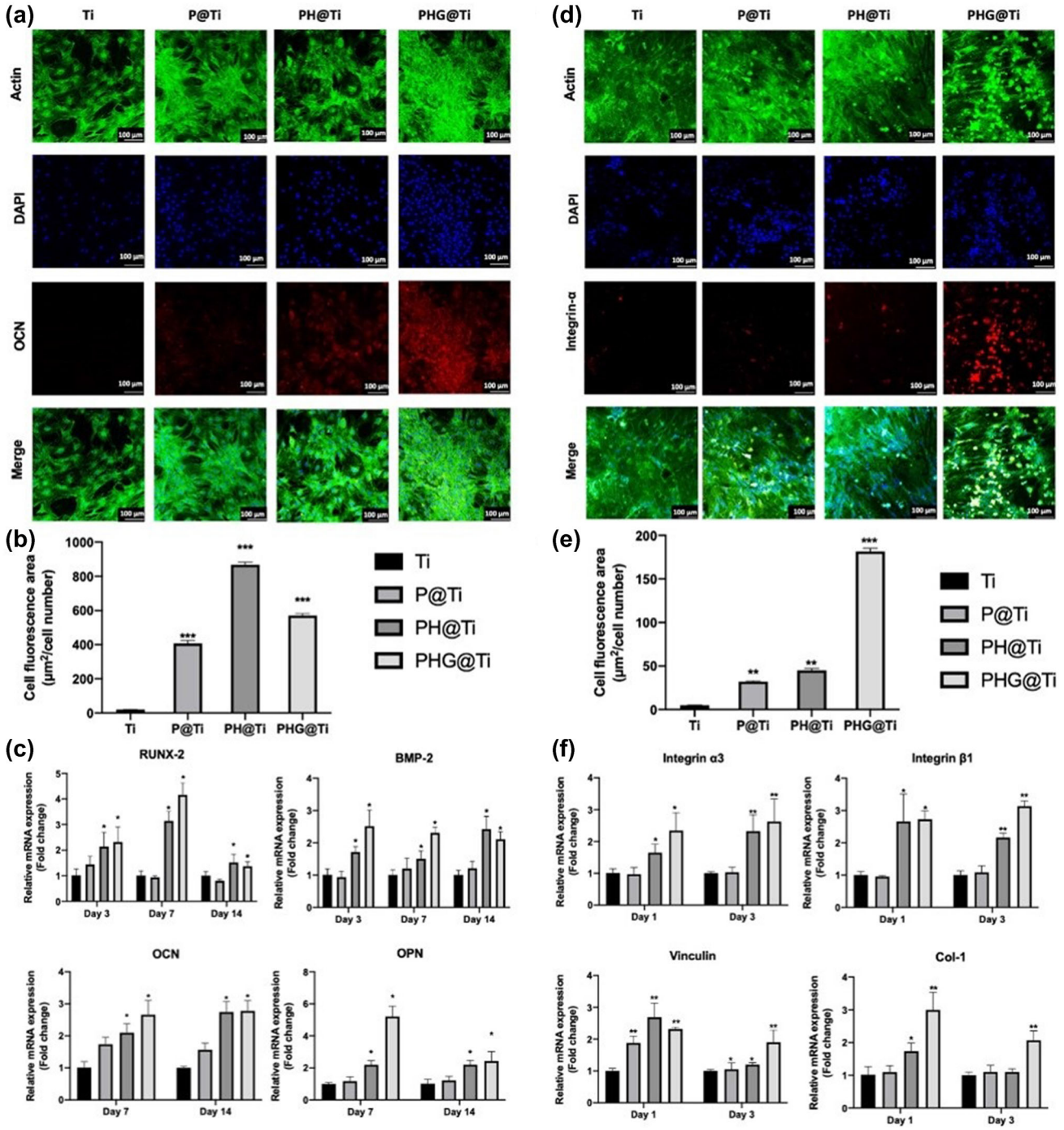

Fig. 6 Immunofluorescence staining results. **a** Expression and **b** statistics of OCN protein (red) detected by immunofluorescence staining. **d** Integrin α protein (red) and **e** its statistics detected by fluorescence staining. Green: actin cytoskeleton; blue: nuclei; yellow: merged color of green and red. **c** Real-time PCR detection of osteogenic genes of BMSCs cultured on samples for 3, 7, and 14 days showing the statistical analyses. **f** Real-time PCR detection of adherence-related genes of HGFs cultured on samples for 1 and 3 days showing the statistical analyses (compared with the Ti group, * $p < 0.05$, ** $p < 0.01$, *** $p < 0.001$)

ALP expression is an early marker of osteogenesis, and ALP activity reflects the ability of osteoblasts to synthesize type I collagen and form a bone matrix [35–37]. During the semi-quantitative determination of ALP activity, the results were calculated by standardizing the protein content. BMSCs cultured in the PHG group showed the highest ALP activity, which was almost five times that of the Ti group (Fig. 7a). Moreover, the ALP activity of BMSCs on Ti-based coating

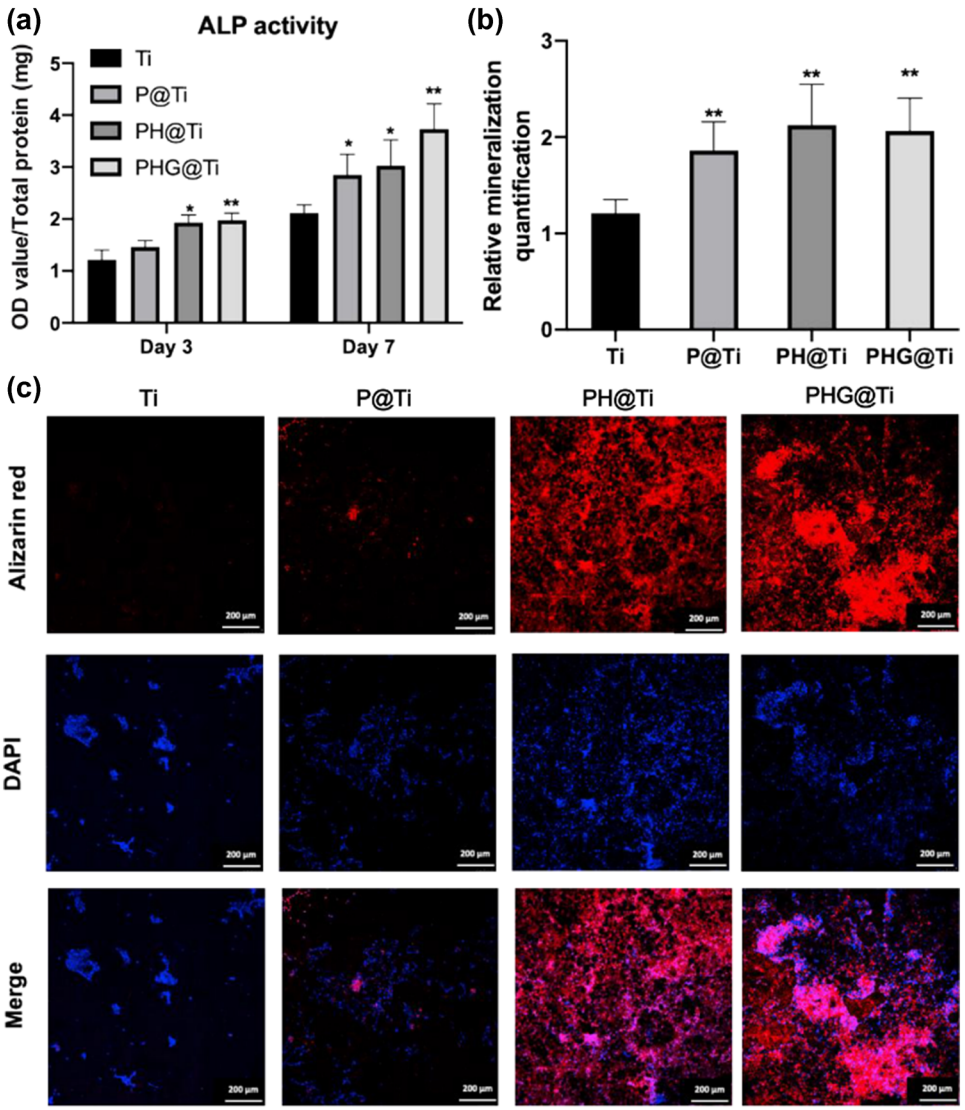

Fig. 7 **a** ALP and **b** ARS semi-quantitative analyses of BMSCs seeded on different samples. **c** Calcium deposition assay. After the BMSCs were cultured for 21 days, ARS staining was performed on all samples. Red fluorescence represents calcium deposition, and the nuclei appear blue (compared with the Ti group, * $p < 0.05$, ** $p < 0.01$)

was related to HA, PDA, and gelatin modification, with significantly higher ALP activity of PH@Ti and PHG@Ti than that of Ti. As shown in Figs. 7b and 7c, the alizarin red-stained regions in the P@Ti, PH@Ti, and PHG@Ti groups were more evident than those in the Ti group, indicating that calcium deposition increased and was consistent with the ALP results. These findings showed that Ti in the PHG coating exhibited biological activity, thus promoting osteogenesis.

Evaluation of antibacterial activity of the modified Ti coatings

The number of viable *S. mutans* on P@Ti, PH@Ti, and PHG@Ti after 24 h of culture was markedly lower than that grown on the pure Ti sample (Fig. 8a). As shown in Figs. 8a and 8b, large numbers of bacteria on PHG@Ti were alive after incubation for 24 h; conversely, most of the bacteria on pure Ti were dead as viable bacteria fluorescing in green were few.

In addition to the stress induced at the alveolar ridge, bone loss around the endosseous dental implants can also result from plaque accumulation on the neck of implants. Compared to natural teeth, dental implants are more prone to bacterial infection that will cause bone loss around the implant, which lacks a periodontal ligament as a protective barrier. Thus, the inclusion of antibacterial materials in the implant design is essential to significantly reduce the rate of peri-implant infections. In fact, our results show that PHG coating not only promoted the growth of HGFs, but also exhibited antibacterial properties. Gao et al. [38] presented a hydrogel system containing PDA nanoparticles, which can not only release antibacterial drugs under NIR, but also the

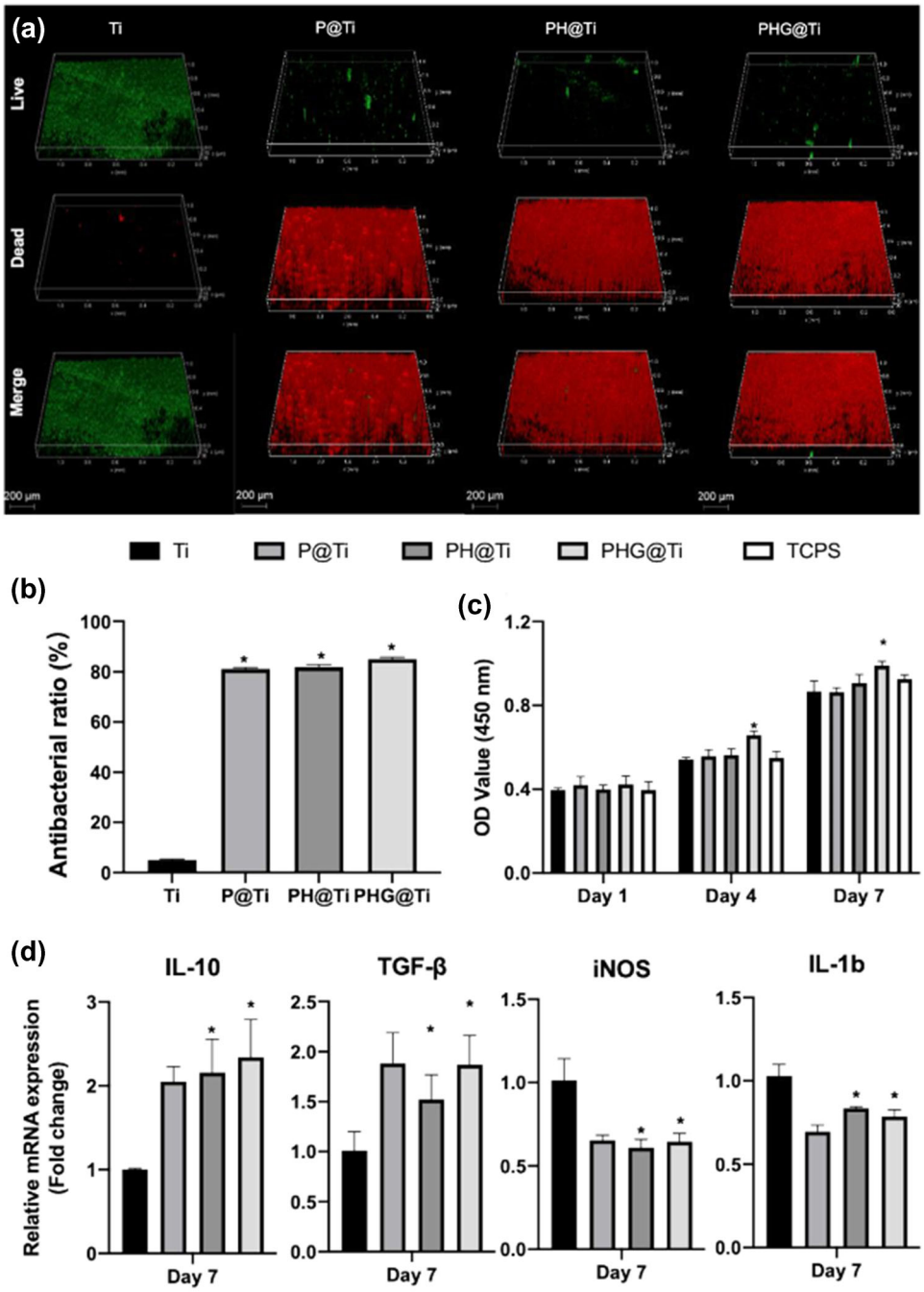

Fig. 8 **a** Dead/live bacteria staining and **b** statistical analyses of bacteria cultured on modified Ti coatings. **c** CCK-8 assay of Raw 264.7 cells and **d** Real-time PCR detection of immune-related genes of Raw 264.7 on the modified Ti coatings (compared with the Ti group, * $p < 0.05$)

polydopamine with good photothermal effect can generate high enough temperature to kill bacteria, thereby enhancing its antibacterial properties. Other than the effect of PDA, the decreased number of adhesive bacteria on the PHG surface might be attributed to the presence of 20-nm nanoparticles that inhibit the preliminary steps of bacterial adhesion by reducing the available substrate-bacteria contact area. This is in accordance with the discovery of Yao et al. [39], who demonstrated that the nanoscale structure (< 100 nm) inhibits bacterial adhesion.

Effects of the modified Ti coatings on the cell behavior of macrophages

In order to simulate the inflammatory microenvironment created by macrophages under the influence of Ti, P@Ti, PH@Ti, and PHG@Ti samples, RAW 264.7 cells were cultured on P@Ti, PH@Ti, and PHG@Ti. The CCK assay (Fig. 8c) showed that, compared with the control group (TCP), the four groups of Ti samples had good biocompatibility and no cytotoxicity.

The relative expression of inflammatory gene markers associated with the M1 (iNOS, IL-1β) and M2 (IL-10, TGF-β) macrophage phenotypes was assessed by quantitative RT-PCR (Fig. 8d). The cytokines linked with the M1 phenotype are generally considered pro-inflammatory factors with important roles in mediating the acute reaction to tissue injury following initial implant insertion, creating an inflammatory microenvironment that initiates the bone healing cascade [40]. Meanwhile, the cytokines associated with the M2 phenotype are considered proregenerative factors that help to create an osteogenic microenvironment conducive to tissue repair, including bone formation and remodeling [41]. After 7 days of culture, the results showed that P@Ti, PH@Ti, and PHG@Ti upregulated the expression of IL-10 and TGF-β, and downregulated the expression of iNOS and IL-1β compared to the Ti groups, particularly at 7 days (Fig. 8d). This pattern of gene expression was consistent with the transition from M1 to M2 phenotype. TNF-α and IL-1β induce an inflammatory response during the early stage of the healing process and can promote macrophage colony-stimulating factor (MCSF) secretion in osteoblasts, which has a role in cell recruitment [42]. Thus, when applied in the short-term at a high dose, these factors can have a positive regulatory effect on osteogenesis [43]. Collectively, the results of PCR suggested that PDA may regulate the polarization of M2 macrophages toward promoting osteogenesis.

Conclusions

In this study, PHG coating was successfully prepared on a porous titanium substrate after alkali heat treatment. This coating showed superior hydrophilic properties and good wettability for cell adhesion. Furthermore, the biological test results confirmed that HGF improved the expression of adhesion-related genes and proteins on the PHG coating surface. Moreover, when BMSCs were cultured on the PHG-coated Ti, the osteogenic gene and protein expressions were upregulated and the mineralized calcium nodules increased, indicating that BMSCs had a strong osteogenic differentiation potential and good mineralization performance on the PHG coating surface. The results also suggested that the PHG coating may help to modulate the osteoimmune response by regulating macrophages in the direction of promoting osteogenesis. The PHG coating exhibited a great photothermal effect, which leads to antibacterial activities against *S. mutans*. These results may contribute to the design of a novel coating structure using PDA/HA nanoparticles with gelation and represent a new strategy for the surface modification of implants.

Supplementary Information The online version contains supplementary material available at https://doi.org/10.1007/s42242-022-00184-5.

Acknowledgements This research was funded by the National Natural Science Foundation of China (Nos. 81801006, 31870953, 81901048, 81620108006, 81991505, 81921002, 81801023, and 82100963), Shanghai Rising-Star Program (21QA1405400), the National Key Research and Development Program of China (No. 2016YFC1102900), and Innovative Research Team of High-Level Local Universities in Shanghai (No. SSMU-ZDCX20180900).

Author contributions Conceptualization, XZX and AZ; methodology, TSS; software, XW; data curation, LJP; writing—original draft preparation, AZ; writing—review and editing, LYC; visualization, AZ and JW; funding acquisition, XZX and XQJ. All authors have read and agreed to the published version of the manuscript.

Declarations

Conflict of interest The authors declare that there were no financial or non-financial interests that are directly or indirectly related to the work submitted for publication.

Ethical approval All institutional and national guidelines for the care and use of laboratory animals were followed. All experimental protocols involving animals were approved by the Institutional Animal Care and Use Committee and followed the procedure for Animal Experimental Ethical Inspection of the Ninth People's Hospital, which is affiliated with Shanghai Jiao Tong University School of Medicine (SCXK (Shanghai) [201866]).

References

1. Papathanasiou E, Finkelman M, Hanley J et al (2016) Prevalence, etiology and treatment of peri-implant mucositis and peri-implantitis: a survey of periodontists in the United States. J Periodontol 87(5):493–501. https://doi.org/10.1902/jop.2015.150476
2. Parma-Benfenati S, Roncati M, Tinti C (2013) Treatment of peri-implantitis: surgical therapeutic approaches based on peri-implantitis defects. Int J Periodontics Restor Dent 33(5):627–633
3. Das S, Dholam K, Gurav S et al (2019) Accentuated osseointegration in osteogenic nanofibrous coated titanium implants. Sci Rep 9(1):17638. https://doi.org/10.1038/s41598-019-53884-x
4. Nishiguchi S, Nakamura T, Kobayashi M et al (1999) The effect of heat treatment on bone-bonding ability of alkali-treated titanium. Biomaterials 20(5):491–500. https://doi.org/10.1016/s0142-9612(98)90203-4
5. Hoppe A, Will J, Detsch R et al (2014) Formation and in vitro biocompatibility of biomimetic hydroxyapatite coatings on chemically treated carbon substrates. J Biomed Mater Res A 102(1):193–203. https://doi.org/10.1002/jbm.a.34685
6. Iezzi G, Scarano A, Petrone G et al (2007) Two human hydroxyapatite-coated dental implants retrieved after a 14-year loading period: a histologic and histomorphometric case report. J Periodontol 78(5):940–947. https://doi.org/10.1902/jop.2007.060271
7. Pang X, Huang Y (2012) Physical properties of nano-HAs/ZrO_2 coating on surface of titanium materials used in dental-implants and its biological compatibility. J Nanosci Nanotechnol 12(2):902–910. https://doi.org/10.1166/jnn.2012.5666
8. Yazdani J, Ahmadian E, Sharifi S et al (2018) A short view on nanohydroxyapatite as coating of dental implants. Biomed Pharmacother 105:553–557. https://doi.org/10.1016/j.biopha.2018.06.013

9. Lowe B, Venkatesan J, Anil S et al (2016) Preparation and characterization of chitosan-natural nano hydroxyapatite-fucoidan nanocomposites for bone tissue engineering. Int J Biol Macromol 93(Pt B):1479–1487. https://doi.org/10.1016/j.ijbiomac.2016.02.054
10. Xu Q, Xu M, Lin CY et al (2019) Metal coordination-mediated functional grading and self-healing in mussel byssus cuticle. Adv Sci (Weinh) 6(23):1902043. https://doi.org/10.1002/advs.201902043
11. Carter PH, Scherle PA, Muckelbauer JK et al (2001) Photochemically enhanced binding of small molecules to the tumor necrosis factor receptor-1 inhibits the binding of TNF-alpha. Proc Natl Acad Sci USA 98(21):11879–11884. https://doi.org/10.1073/pnas.21117839812
12. Meyle J (2012) Mechanical, chemical and laser treatments of the implant surface in the presence of marginal bone loss around implants. Eur J Oral Implantol 5(Suppl):S71–S81
13. Wang M, Wu H, Li Q et al (2019) Novel aptamer-functionalized nanoparticles enhances bone defect repair by improving stem cell recruitment. Int J Nanomed 14:8707–8724. https://doi.org/10.2147/IJN.S223164
14. Yoshinari M, Hayakawa T, Matsuzaka K et al (2006) Oxygen plasma surface modification enhances immobilization of simvastatin acid. Biomed Res 27(1):29–36. https://doi.org/10.2220/biomedres.27.29
15. Fassina L, Saino E, Visai L et al (2010) Use of a gelatin cryogel as biomaterial scaffold in the differentiation process of human bone marrow stromal cells. Annu Int Conf IEEE Eng Med Biol Soc 2010:247–250. https://doi.org/10.1109/IEMBS.2010.5627475
16. Yang F, Zhao SF, Zhang F et al (2011) Simvastatin-loaded porous implant surfaces stimulate preosteoblasts differentiation: an in vitro study. Oral Surg Oral Med Oral Pathol Oral Radiol Endod 111(5):551–556. https://doi.org/10.1016/j.tripleo.2010.06.018
17. Wu J, Zheng A, Liu Y et al (2019) Enhanced bone regeneration of the silk fibroin electrospun scaffolds through the modification of the graphene oxide functionalized by BMP-2 peptide. Int J NanoMed 14:733–751. https://doi.org/10.2147/IJN.S187664
18. Wu J, Cao L, Liu Y et al (2019) Functionalization of silk fibroin electrospun scaffolds via BMSC affinity peptide grafting through oxidative self-polymerization of dopamine for bone regeneration. ACS Appl Mater Interf 11(9):8878–8895. https://doi.org/10.1021/acsami.8b22123
19. Jiao D, Cao L, Liu Y et al (2019) Synergistic osteogenesis of biocompatible reduced graphene oxide with methyl vanillate in BMSCs. ACS Biomater Sci Eng 5(4):1920–1936. https://doi.org/10.1021/acsbiomaterials.8b01264
20. He J, Zhu X, Qi Z et al (2015) Killing dental pathogens using antibacterial graphene oxide. ACS Appl Mater Interf 7(9):5605–5611. https://doi.org/10.1021/acsami.5b01069
21. Shibata Y, Suzuki D, Omori S et al (2010) The characteristics of in vitro biological activity of titanium surfaces anodically oxidized in chloride solutions. Biomaterials 31(33):8546–8555. https://doi.org/10.1016/j.biomaterials.2010.07.098
22. Chen TW, Ramachandran R, Chen SM et al (2020) Graphene and perovskite-based nanocomposite for both electrochemical and gas sensor applications: an overview. Sensors (Basel) 20(23):6755. https://doi.org/10.3390/s20236755
23. Ho CC, Ding SJ (2013) The pH-controlled nanoparticles size of polydopamine for anti-cancer drug delivery. J Mater Sci Mater Med 24(10):2381–2390. https://doi.org/10.1007/s10856-013-4994-2
24. Saita M, Ikeda T, Yamada M, Kimoto K, Lee MC, Ogawa T (2016) UV photofunctionalization promotes nano-biomimetic apatite deposition on titanium. Int J Nanomed 11:223–234
25. Lu M, Chen H, Yuan B, Zhou Y, Min L, Xiao Z et al (2020) Electrochemical deposition of nanostructured hydroxyapatite coating on titanium with enhanced early stage osteogenic activity and osseointegration. Int J Nanomed 15:6605–6618
26. Ma H, Luo J, Sun Z et al (2016) 3D printing of biomaterials with mussel-inspired nanostructures for tumor therapy and tissue regeneration. Biomaterials 111:138–148. https://doi.org/10.1016/j.biomaterials.2016.10.005
27. Mezu-Ndubuisi OJ, Maheshwari A (2021) The role of integrins in inflammation and angiogenesis. Pediatr Res 89(7):1619–1626. https://doi.org/10.1038/s41390-020-01177-9
28. Tian J, Zhang FJ, Lei GH (2015) Role of integrins and their ligands in osteoarthritic cartilage. Rheumatol Int 35(5):787–798. https://doi.org/10.1007/s00296-014-3137-5
29. Ye J, Huang B, Gong P (2021) Nerve growth factor-chondroitin sulfate/hydroxyapatite-coating composite implant induces early osseointegration and nerve regeneration of peri-implant tissues in Beagle dogs. J Orthop Surg Res 16(1):51. https://doi.org/10.1186/s13018-020-02177-5
30. Karimi Z, Ghorbani M, Hashemibeni B et al (2015) Evaluation of the proliferation and viability rates of nucleus pulposus cells of human intervertebral disk in fabricated chitosan-gelatin scaffolds by freeze drying and freeze gelation methods. Adv Biomed Res 4:251. https://doi.org/10.4103/2277-9175.170676
31. Saidin S, Chevallier P, Abdul KM et al (2013) Polydopamine as an intermediate layer for silver and hydroxyapatite immobilisation on metallic biomaterials surface. Mater Sci Eng C Mater Biol Appl 33(8):4715–4724. https://doi.org/10.1016/j.msec.2013.07.026
32. Sang L, Huang J, Luo D et al (2010) Bone-like nanocomposites based on self-assembled protein-based matrices with Ca^{2+} capturing capability. J Mater Sci Mater Med 21(9):2561–2568. https://doi.org/10.1007/s10856-010-4117-2
33. Yu P, Bao RY, Shi XJ et al (2017) Self-assembled high-strength hydroxyapatite/graphene oxide/chitosan composite hydrogel for bone tissue engineering. Carbohydr Polym 155:507–515. https://doi.org/10.1016/j.carbpol.2016.09.001
34. Fukuda A, Takemoto M, Saito T et al (2011) Bone bonding bioactivity of Ti metal and Ti-Zr-Nb-Ta alloys with Ca ions incorporated on their surfaces by simple chemical and heat treatments. Acta Biomater 7(3):1379–1386. https://doi.org/10.1016/j.actbio.2010.09.026
35. Cosmidis J, Benzerara K, Nassif N et al (2015) Characterization of Ca-phosphate biological materials by scanning transmission X-ray microscopy (STXM) at the Ca L2,3-, P L2,3- and C K-edges. Acta Biomater 12:260–269. https://doi.org/10.1016/j.actbio.2014.10.003
36. Lim ZW, Chen WL (2020) Exploring the association of bone alkaline phosphatases and hearing loss. Sci Rep 10(1):4006. https://doi.org/10.1038/s41598-020-60979-3
37. Trowsdale J, Martin D, Bicknell D et al (1990) Alkaline phosphatases. Biochem Soc Trans 18(2):178–180. https://doi.org/10.1007/s11302-005-5435-6
38. Gao G, Jiang YW, Jia HR et al (2019) Near-infrared light-controllable on-demand antibiotics release using thermo-sensitive hydrogel-based drug reservoir for combating bacterial infection. Biomaterials 188:83–95. https://doi.org/10.1016/j.biomaterials.2018.09.045
39. Yao C, Webster TJ, Hedrick M (2014) Decreased bacteria density on nanostructured polyurethane. J Biomed Mater Res A 102(6):1823–1828. https://doi.org/10.1002/jbm.a.34856
40. Gao Q, Rhee C, Maruyama M et al (2021) The effects of macrophage phenotype on osteogenic differentiation of MSCs in the presence of polyethylene particles. Biomedicines 9(5):499. https://doi.org/10.3390/biomedicines9050499
41. Xu R, Shen X, Si Y et al (2018) MicroRNA-31a-5p from aging BMSCs links bone formation and resorption in the aged bone marrow microenvironment. Aging Cell 17(4):e12794. https://doi.org/10.1111/acel.12794

42. Sun H, Dai K, Tang T et al (2009) Regulation of osteoblast differentiation by slit2 in osteoblastic cells. Cells Tissues Organs 190(2):69–80. https://doi.org/10.1159/000178020

43. Darcy A, Meltzer M, Miller J et al (2012) A novel library screen identifies immunosuppressors that promote osteoblast differentiation. Bone 50(6):1294–1303. https://doi.org/10.1016/j.bone.2012.03.001